ACS SENSORS

Article

pubs.acs.org/acssensors

Long-Term Stability of Oxide Nanowire Sensors via Heavily Doped Oxide Contact

Hao Zeng,[†] Tsunaki Takahashi,*[,†] Masaki Kanai,[†] Guozhu Zhang,[†] Yong He,[‡] Kazuki Nagashima,[†] and Takeshi Yanagida*[,†]

[†]Institute for Materials Chemistry and Engineering, Kyushu University, 6-1 Kasuga-Koen, Kasuga, Fukuoka 816-8580, Japan

[‡]Key Laboratory of Optoelectronic Technology and Systems of the Education Ministry of China, Chongqing University, Chongqing 400044, P. R. China

Supporting Information

ABSTRACT: Long-term stability of a chemical sensor is an essential quality for long-term collection of data related to exhaled breath, environmental air, and other sources in the Internet of things (IoT) era. Although an oxide nanowire sensor has shown great potential as a chemical sensor, the long-term stability of sensitivity has not been realized yet due to electrical degradation under harsh sensing conditions. Here, we report a rational concept to accomplish long-term electrical stability of metal oxide nanowire sensors via introduction of a heavily doped metal oxide contact layer. Antimony-doped SnO_2 (ATO) contacts on SnO_2 nanowires show much more stable and lower electrical contact resistance than conventional Ti contacts for high temperature (200 °C) conditions, which are required to operate chemical sensors. The stable and low contact resistance of ATO was confirmed for at least 1960 h under 200 °C in open air. This heavily doped oxide contact enables us to realize the long-term stability of SnO_2 nanowire sensors while maintaining the sensitivity for both NO_2 gas and light (photo) detections. The applicability of our method is confirmed for sensors on a flexible polyethylene naphthalate (PEN) substrate. Since the proposed fundamental concept can be applied to various oxide nanostructures, it will give a foundation for designing long-term stable oxide nanomaterial-based IoT sensors.

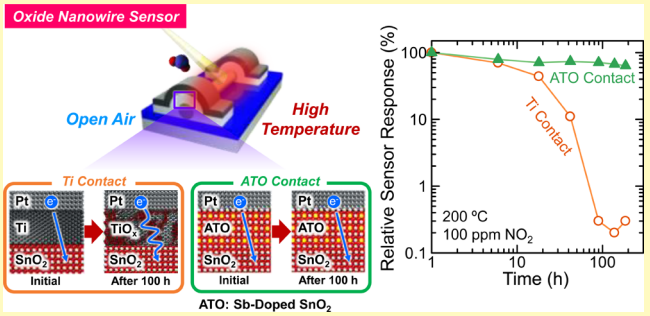

KEYWORDS: *long-term stability, oxide nanowire, chemical sensor, contact resistance, SnO_2*

Electronics-based chemical sensors have attracted significant attention as a key device of Internet of things (IoT) technology toward a breath diagnosis,[1−4] detection of explosives and toxic substances,[5−7] and industrial/agricultural production control.[8−10] For these chemical sensors, long-term stability of the sensor response is an essential requirement for time-series data collection and big data analysis. However, obtaining such long-term stability of chemical sensors is inherently difficult when compared with conventional electron devices such as transistors and memory, which can be passivated. This is because chemical sensors must be exposed to ambient air for molecular detection in the surrounding space, which can substantially alter the electrical properties of sensors from initially designed electrical conditions. Since, in general, highly sensitive sensors exhibit less long-term stability due to the chemical reactions to air/humidity in surroundings, the compatibility of sensitivity and long-term stability is a fundamental and important challenge for chemical sensors in IoT technology.

Among various functional nanomaterials, metal oxide nanowires have shown excellent properties as chemical sensors.[11,12] This is because metal oxide nanowires can exhibit relatively wide control of chemical reactivity via altering metal ions, large surface/volume ratio, chemical stability to surrounding air, and other factors.[13−16] In previous studies regarding nanowire-based sensor devices, major attention/effort has been directed to studying the electrical characteristics and sensing properties rather than the long-term stability. The electrical stability of metal oxide nanowire devices (transistors) has been reported by introducing passivation layers such as inorganic material,[17] polymer,[18,19] and self-assembled monolayer (SAM).[20] However, these conventional strategies using passivation layers are essentially not applicable to chemical sensors, because sensor devices must be exposed to analytes in the surroundings.

In nanoscale electron channel devices, energy barriers and carrier scatterings at boundaries mainly limit the carrier transport.[21−23] In particular, electrical contacts between electrodes and channels have significant impacts on device performance of a single crystalline nanowire which has no grain boundary in the channel.[24,25] Reliable electrical contacts on

Received: September 25, 2017
Accepted: October 23, 2017
Published: October 23, 2017

DOI: 10.1021/acssensors.7b00716
ACS Sens. 2017, 2, 1854−1859

semiconductor nanowires have been widely investigated typically via Ohmic contacts between metal and silicon nanowires.[26−28] For metal oxide nanowires, several issues have been reported such as oxidation at electrode/nanowire interface,[29] interface trap states,[30] and change in surface stoichiometry.[31] The general concepts to obtain reliable and low-resistance electrical contacts are twofold: one is lowering a Schottky barrier height at the interface by the energy level matching the work function of electrodes and the Fermi level in semiconductor channels; the other is enhancing the tunneling probability of carriers through the Schottky barrier using degenerate, namely, highly doped, semiconductor at the electrode/semiconductor interface. The former concept has been adopted in metal oxides for many years. Since most binary oxide semiconductors are n-type doped due to stoichiometric deviations and/or interstitial ions,[32−36] low work function metals such as Ti, Cr, and Al are generally selected as a contact electrode material to metal oxides.[37] Among these metals, Ti electrode has been most widely used for typical metal oxide (e.g., SnO_2, ZnO) devices by taking into account the energy level matching and good adhesion to the substrate.[38] However, these low work function metals are easily oxidized in high temperature oxygen atmosphere, which corresponds to the operation conditions of conventional metal oxide sensors.[29] Although the contact metal oxidation increases contact resistance and degrades sensor performance after long-term operations, these low function metal contacts have been employed in oxide-based sensors due to the absence of alternative methodology for electrical contacts. Thus, these inherent electrical contact issues for metal oxides mainly have inhibited the long-term stability of oxide nanowire sensors during high temperature operations without passivation layers.

In this work, we propose a rational concept to obtain long-term stability of metal oxide nanowire sensors via introducing stable and low resistance contact on oxide nanowires using heavily doped metal oxides as a contact material (Figure 1a). Antimony-doped SnO_2 (ATO) contact enables at least 1960 h electrical stability of SnO_2 nanowires at 200 °C in air, whereas conventional Ti contact devices exhibited significant electrical degradation in contact resistance within several hours. The excellent characteristics of ATO contact after the long-term heating can be interpreted in terms of the energy band diagram of electrode/ATO/SnO_2 nanowire stack system. The sensor responses after long-term operations (NO_2 and photo detections) are dramatically improved by utilizing the ATO contact, indicating practical advantages of the concept. The ATO contacts are also performed for nanowire devices on a polyethylene naphthalate (PEN) substrate which has attracted growing attention as flexible-electronic-based wearable sensors.[39,40]

EXPERIMENTAL SECTION

SnO_2 Nanowire Growth. Pulsed laser deposition (PLD) technique was applied to grow SnO_2 nanowires via a vapor−liquid−solid (VLS) process on an Al_2O_3 (110) single crystalline substrate.[41,42] First, 0.7 nm Au film was deposited on the Al_2O_3 substrate using DC sputtering and annealing at 750 °C for 10 min to form agglomerated Au nanoparticle catalysts. Second, SnO_2 nanowires were grown at 750 °C in 10 Pa of oxygen/argon mixed gas (O_2:Ar = 1:1000) by an ArF excimer laser (Coherent COMPex-Pro, λ = 193 nm) ablation with the following conditions: pulse repetition time of 10 Hz and laser energy of 40 mJ. SnO_2 mixed with Sb_2O_3 (0.5 atomic %) target was used as the source of Sn. The grown nanowires were characterized by a field emission scanning electron microscope (FESEM) and the diameters of the nanowires were around 50 nm.

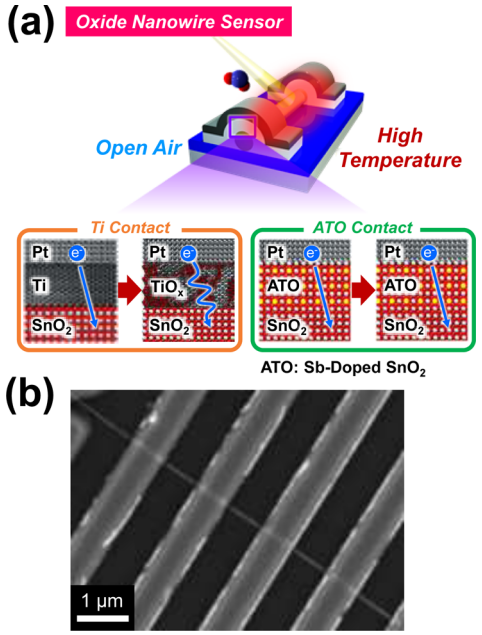

Figure 1. (a) Concept to achieve long-term stability and low resistance electrical contact on metal oxide nanowires. (b) Field emission scanning electron microscope (FESEM) image of a typical fabricated four-terminal nanowire device.

Device Fabrication. The grown SnO_2 nanowires were first treated by ultrasonic dispersion in isopropanol and dropped on a 100 nm SiO_2/n-type Si substrate. Electrode patterning was performed using electron-beam lithography and lift-off techniques. For Ti contact devices, Ti/Pt of 20/100 nm was deposited using radiofrequency (RF) sputtering. For ATO contact devices, ATO/Pt of 20/100 nm was deposited using PLD and RF sputtering at room temperature, respectively. A SnO_2 mixed with Sb_2O_3 (10 atomic %) target was used in ATO depositions. Finally, ATO contact devices were annealed at 700 °C for 10 min in 10 Pa Ar atmosphere. A FESEM image of a typical fabricated device is shown in Figure 1b. Channel length, as well as the separation between electrodes, is 1 μm for each device. For the devices on PEN substrates, annealing after ATO deposition was performed at 200 °C for 10 min. It is noted that thermal annealing was needed for ATO contact devices to lowering the resistance of ATO film (see Figure S1 in the Supporting Information).

Electrical Characterizations. All electrical characteristics were measured using a semiconductor parameter analyzer (Keithley 4200 SCS) with a probe station including a hot chuck in an ambient pressure. The contact resistance (R_c) was extracted as $R_c = R_{2p} - R_{4p}$. Here, R_{2p} and R_{4p} are resistances measured by the two- and four-probe techniques, respectively. In the molecular detections, N_2 balanced 100 ppm of NO_2 was introduced in a chamber. Photoresponse characteristics were evaluated using a UV light source (λ = 260 nm) in ambient air. For the NO_2 sensing and photodetecting measurements, the resistance of nanowires under dry air flow and dark condition was defined as R_0. The sensor response was extracted as $(R/R_0) \times 100\%$. Here, R is the resistance of nanowires. All the stability evaluation experiments were performed by heating the devices at 200 °C in open air (humidity of around 40%) during intervals between electrical measurements. The NO_2 sensing characteristics were measured at 200 °C and the others were measured at room temperature. A more detailed extraction method of the contact resistance and sensing response can be found in the Supporting Information.

DOI: 10.1021/acssensors.7b00716
ACS Sens. 2017, 2, 1854−1859

RESULTS AND DISCUSSION

Figure 1a illustrates our strategy to obtain long-term stability of metal oxide nanowire sensors via reliable and good electrical contacts on metal oxide nanowires for SnO_2 nanowires. A heavily doped metal oxide film is used as a contact layer on metal oxide nanowires because metal oxides show superior chemical stability at a high temperature in an oxygen and humid atmosphere.[43,44] The strong doping is necessary to achieve a low and thin Schottky barrier, namely, lower contact resistance between electrodes and oxides as discussed later. Figure 2a,b shows the two-probe $I-V$ characteristics of Ti and ATO contact nanowires during long-term thermal treatments (200 °C, open air). Although the conventional Ti contact device shows good linear Ohmic characteristics and sufficiently low resistance just after fabrication (indicated as "Initial" in Figure 2a), the resistance drastically increases as time goes by. These results indicate that the widely used Ti contacts fail to ensure reliable high-temperature operations for sensors. On the other hand, the ATO contact device maintains a good linearity of $I-V$ curves with only a slight increase in resistance. It should be noted that ATO contact devices have a high resistance just after ATO layer deposition (indicated as dashed line and "before Annealing" in Figure 2b). The electrical resistivity of the ATO film greatly decreases by thermal annealing (Figure S1). The thermal stress tests ("Initial, 6 h, 1960 h" in Figure 2b) were performed after the thermal annealing.

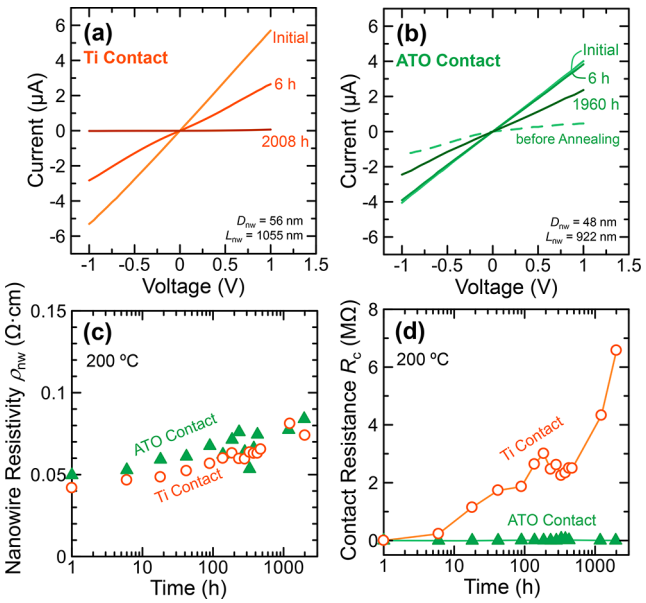

Figure 2. $I-V$ characteristics of (a) Ti and (b) heavily antimony-doped SnO_2 (ATO) contact SnO_2 nanowire devices measured by two-probe technique. $I-V$ characteristics as fabricated (initial) and after heating at 200 °C in open air (6 and 2008 h for Ti contact, 6 and 1960 h for ATO contact) are shown. For the ATO contact device, $I-V$ characteristics before annealing (700 °C, 10 min) are also shown. (c) Relationship between nanowire resistivity (ρ_{nw}) and duration of the heating (200 °C, open air) for Ti and ATO contact devices. (d) Relationship between contact resistance (R_c) and duration of heating for Ti and ATO contact devices.

Next, we reveal the origin of the difference between Ti and ATO electrical contacts of two-probe measurements in Figure 2a,b. Since the measured two-probe electrical resistance essentially includes nanowire resistivity (ρ_{nw}) and contact resistance (R_c), we distinguish these two contributions on the present devices by performing four-probe measurements through the heating, as shown in Figure 2c,d. As seen, the ρ_{nw} slightly increases in both the Ti and ATO contact devices due to the compensation of oxygen vacancies in SnO_2 nanowires which suppress mobile electrons.[45] The ρ_{nw} increase results in the slight current decrease observed for ATO contact devices. In contrast, the variations of R_c are quite different between the Ti and ATO contacts. The rapid increase in R_c of Ti contacts was clearly observed during less than 200 h heating, whereas the R_c of ATO contact is almost constant over 1960 h. Thus, the advantage of ATO contacts compared to the conventional Ti contacts is clearly shown in terms of the thermal stability of contact resistance R_c.

The rapid increase in R_c of Ti contact is due to the oxidation of Ti. Just after fabrication, Ti and n-type SnO_2 form a good Ohmic contact due to their band alignment (Figure 3a). However, Ti is gradually oxidized to TiO_x under high temperature and oxygen atmosphere.[46,47] Therefore, the contact stack is altered to $Pt/TiO_x/SnO_2$ in the case of our devices. Because of the low work function and semiconducting features of TiO_x,[48,49] a high and thick Schottky barrier is formed between SnO_2 nanowire and Pt (electrodes) including barriers at Pt/TiO_x and TiO_x/SnO_2 as shown in Figure 3b, resulting in the R_c increase of Ti contact devices under heating. In fact, the $I-V$ curves of Ti contact devices show Schottky diode like characteristics after heating (see Figure S2 in the Supporting Information). The similar Schottky diode like characteristics of Ti contact devices have been reported for InP nanowire sensor devices.[50] For ATO contacts, thanks to the perfect band alignment at ATO/SnO_2 nanowires and extremely thin Schottky barrier between n+ ATO/Pt, electrons can easily

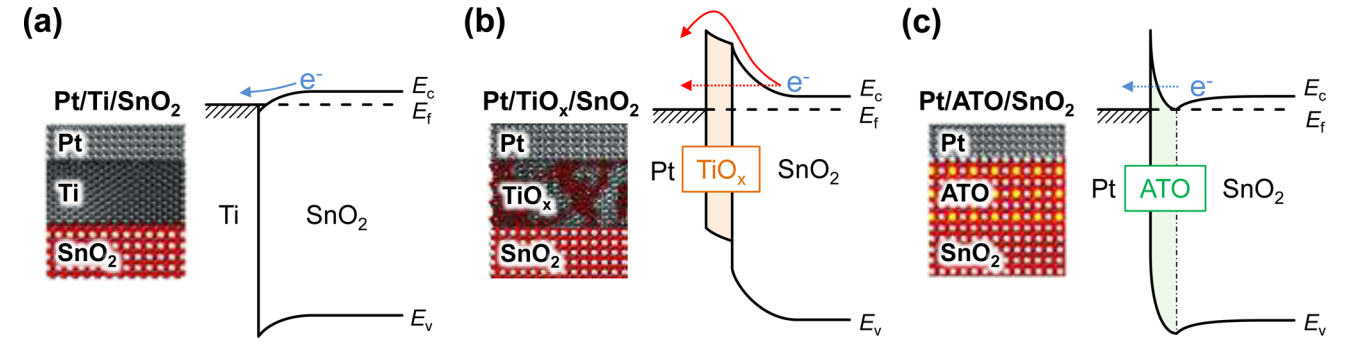

Figure 3. Energy band diagrams at cross sections between electrode and SnO_2 nanowire channel for (a) Ti/SnO_2, (b) $Pt/TiO_x/SnO_2$, and (c) $Pt/ATO/SnO_2$ stacks.

DOI: 10.1021/acssensors.7b00716
ACS Sens. 2017, 2, 1854−1859

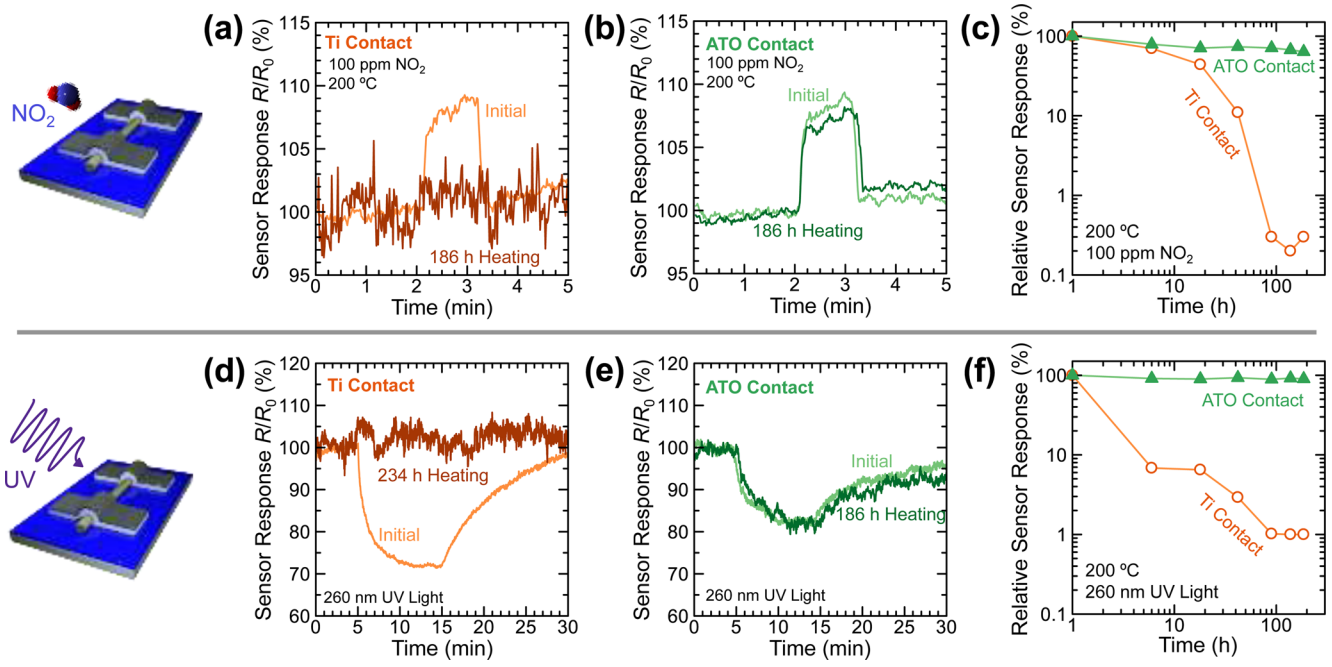

Figure 4. Time-dependent sensing characteristics for Ti and ATO contact devices. (a, b) Resistance change in N_2-balanced 100 ppm of NO_2 atmosphere. (d, e) Resistance change under UV light (260 nm). (c) Relationship between relative sensing response to N_2-balanced 100 ppm of NO_2 and duration of heating (200 °C, open air). (f) Relationship between relative sensing response to UV light (260 nm) and duration of the heating. The response values are normalized by the initial responses.

tunnel through the barrier and low R_c is achieved. More importantly, the good contact characteristics can be maintained even after long-term thermal treatments due to the chemical stability of metal oxide electrode ATO (Figure 2d).

Next we demonstrate the feasibility of ATO contact for long-term stability of metal oxide nanowire sensors under high temperature conditions. Resistance changes under 100 ppm of NO_2 atmosphere and 260 nm UV light were measured for the Ti and ATO contact devices as shown in Figure 4. Obviously, only the response of Ti contact devices tends to degrade after around 200 h of heating time. The significant reduction of the sensor response results from the increase in the R_c of Ti contacts. In general, a sensor response is defined as $R/R_0 = (R_c + R_{nw} + \Delta R_{nw})/(R_c + R_{nw})$, where R_{nw} and ΔR_{nw} are initial nanowire resistance and change in R_{nw} under gas/light, respectively. When the contact resistance is much larger than the nanowire resistance, i.e., $R_c \gg R_{nw}$, the measured sensor signal is determined by R_c, and the sensor response must be negligible. This situation corresponds to the case of the Ti contact devices after heating. To more clearly reveal the electrical degradation of metal oxide nanowire sensors, we estimate the relative response data of sensors, which is defined as (resistance change)/(initial resistance change) × 100. Figure 4c,f shows the time series data of measured relative response values for NO_2/UV light sensing. As can be clearly seen, for both gas and light detections, the response of Ti contact devices rapidly degrades down to less than 1% of initial value within 100 h. On the other hand, the response of ATO contact devices is almost constant and does not deviate from the initial response value within the measured time range. The slight decrease in the response of ATO contact device is presumably due to the change in SnO_2 nanowire surface by oxygen as discussed in Figure 2c. These results highlight that the present strategy using ATO contact greatly enhances the electrical stability of metal oxide nanowire sensors.

Finally, the applicability of the present strategy was confirmed for nanowire devices on a flexible substrate. The ATO contact SnO_2 nanowire devices were fabricated on a polyethylene naphthalate (PEN) substrate by decreasing the annealing temperature after ATO depositions to 200 °C (Figure 5a,b). As shown in Figure 5c,d, the long-term stability of R_c in ATO contact devices was successfully observed even for the flexible PEN substrate. It is noted that the relative low

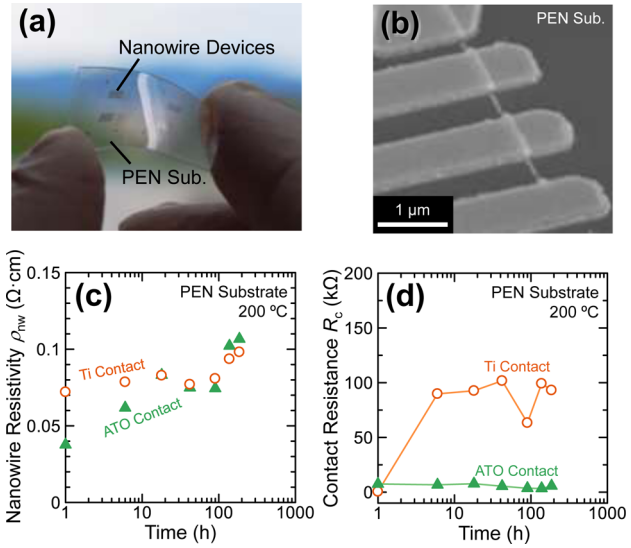

Figure 5. Demonstration of our concept using a flexible polyethylene naphthalate (PEN) substrate. (a) Chip photograph and (b) device FESEM image. (c) Relationship between nanowire resistivity (ρ_{nw}) and duration of the heating (200 °C, open air) for Ti and ATO contact devices. (d) Relationship between contact resistance (R_c) and duration of the heating for Ti and ATO contact devices.

DOI: 10.1021/acssensors.7b00716
ACS Sens. 2017, 2, 1854−1859

R_c of Ti contact devices compared with that on Si substrates is probably due to the thermal decomposition of PEN substrates (see the Supporting Information). Thus, our proposed strategy can be extended for various substrates.

CONCLUSIONS

We demonstrate a rational strategy to achieve long-term stability of metal oxide nanowire sensors by using heavily doped metal oxides as a contact layer, which creates low resistance and thermally stable electrical contact to metal oxide nanowires. The contact resistance (R_c) of conventional Ti contact on SnO_2 nanowires rapidly increased under several hours of 200 °C heating in air due to Ti oxidation, whereas the proposed heavily Sb-doped SnO_2 (ATO) contact maintained sufficiently low R_c for at least 1960 h of heating. The origin of the excellent property of ATO contact is twofold: (1) chemical stability of metal oxides (ATO), and (2) low R_c results from the band alignment between ATO/SnO_2 nanowires and the extremely thin Schottky barrier at ATO/Pt electrodes due to degenerated carrier doping in ATO. The feasibility of our strategy is verified through the evaluation of long-term sensor responses to NO_2 and UV light. Much higher and more stable responses were obtained for ATO contact sensors, directly indicating the practical advantages of our strategy for chemical sensors whose essential requirement is long-term and low-power operations. Finally, the feasibility of present ATO contact for a PEN substrate was successfully demonstrated to validate the compatibility of our concept with wearable sensors. Our present concept will be a foundation to obtain a long-term electrical stability of oxide nanodevices for various metal oxides.

ASSOCIATED CONTENT

Supporting Information

The Supporting Information is available free of charge on the ACS Publications website at DOI: 10.1021/acssensors.7b00716.

Annealing effects on resistivity and morphology of ATO film; extraction of contact resistance and sensor response; current degradation of Ti contact devices under heating; thermal decomposition of PEN substrate (PDF)

AUTHOR INFORMATION

Corresponding Authors

*E-mail: takahashi.t@cm.kyushu-u.ac.jp.
*E-mail: yanagida@cm.kyushu-u.ac.jp.

ORCID

Takeshi Yanagida: 0000-0003-4837-5701

Notes

The authors declare no competing financial interest.

ACKNOWLEDGMENTS

This work was supported by CREST of Japan Science and Technology Corporation (JST). Y. T. was supported by ImPACT. H. Z., T. T., Z. G., Y. H., and K. N were supported by KAKENHI Grant Numbers (No.17H04927, No.26706005, No.16H00969, No.15K13288, No.15H03528, No.26220908). This work was performed under the Cooperative Research Program of "Network Joint Research Center for Materials and Devices" and the MEXT Project of "Integrated Research Consortium on Chemical Sciences".

REFERENCES

(1) Yin, P. T.; Shah, S.; Chhowalla, M.; Lee, K. B. Design, synthesis, and characterization of graphene-nanoparticle hybrid materials for bioapplications. *Chem. Rev.* **2015**, *115*, 2483−2531.

(2) Paska, Y.; Stelzner, T.; Christiansen, S.; Haick, H. Enhanced sensing of nonpolar volatile organic compounds by silicon nanowire field effect transistors. *ACS Nano* **2011**, *5*, 5620−5626.

(3) Peng, G.; Trock, E.; Haick, H. Detecting simulated patterns of lung cancer biomarkers by random network of single-walled carbon nanotubes coated with nonpolymeric organic materials. *Nano Lett.* **2008**, *8*, 3631−3635.

(4) Peng, G.; Tisch, U.; Adams, O.; Hakim, M.; Shehada, N.; Broza, Y. Y.; Billan, S.; Abdah-Bortnyak, R.; Kuten, A.; Haick, H. Diagnosing lung cancer in exhaled breath using gold nanoparticles. *Nat. Nanotechnol.* **2009**, *4*, 669−673.

(5) Lin, Z. H.; Zhu, G.; Zhou, Y. S.; Yang, Y.; Bai, P.; Chen, J.; Wang, Z. L. A Self-powered triboelectric nanosensor for mercury ion detection. *Angew. Chem., Int. Ed.* **2013**, *52*, 5065−5069.

(6) Engel, Y.; Elnathan, R.; Pevzner, A.; Davidi, G.; Flaxer, E.; Patolsky, F. Supersensitive detection of explosives by silicon nanowire arrays. *Angew. Chem., Int. Ed.* **2010**, *49*, 6830−6835.

(7) Lichtenstein, A.; Havivi, E.; Shacham, R.; Hahamy, E.; Leibovich, R.; Pevzner, A.; Krivitsky, V.; Davivi, G.; Presman, I.; Elnathan, R.; Engel, Y.; Flaxer, E.; Patolsky, F. Supersensitive fingerprinting of explosives by chemically modified nanosensors arrays. *Nat. Commun.* **2014**, *5*, 4195.

(8) Neethirajan, S.; Jayas, D. S. Nanotechnology for the food and bioprocessing industries. *Food Bioprocess Technol.* **2011**, *4*, 39−47.

(9) Hart, J. P.; Wring, S. A. Recent developments in the design and application of screen-printed electrochemical sensors for biomedical, environmental and industrial analyses. *TrAC, Trends Anal. Chem.* **1997**, *16*, 89−103.

(10) Birrell, S. J.; Hummel, J. W. Real-time multi ISFET/FIA soil analysis system with automatic sample extraction. *Comput. Electron. Agric.* **2001**, *32*, 45−67.

(11) Shen, Y.; Yamazaki, T.; Liu, Z.; Meng, D.; Kikuta, T.; Nakatani, N.; Saito, M.; Mori, M. Microstructure and H_2 gas sensing properties of undoped and Pd-doped SnO_2 nanowires. *Sens. Actuators, B* **2009**, *135*, 524−529.

(12) Lin, Z.; Li, N.; Chen, Z.; Fu, P. The effect of Ni doping concentration on the gas sensing properties of Ni doped SnO_2. *Sens. Actuators, B* **2017**, *239*, 501−510.

(13) Meng, G.; Zhuge, F.; Nagashima, K.; Nakao, A.; Kanai, M.; He, Y.; Boudot, M.; Takahashi, T.; Uchida, K.; Yanagida, T. Nanoscale thermal management of single SnO_2 nanowire: pico-joule energy consumed molecule sensor. *ACS Sensors* **2016**, *1*, 997−1002.

(14) Kolmakov, A.; Klenov, D. O.; Lilach, Y.; Stemmer, S.; Moskovits, M. Enhanced gas sensing by individual SnO_2 nanowires and nanobelts functionalized with Pd catalyst particles. *Nano Lett.* **2005**, *5*, 667−673.

(15) Hoffmann, M. W. G.; Prades, J. D.; Mayrhofer, L.; Hernandez-Ramirez, F.; Jaervi, T. T.; Moseler, M.; Waag, A.; Shen, H. Highly selective SAM-nanowire hybrid NO_2 sensor: insight into charge transfer dynamics and alignment of frontier molecular orbitals. *Adv. Funct. Mater.* **2014**, *24*, 595−602.

(16) Jeong, S. H.; Kim, S.; Cha, J.; Son, M. S.; Park, S. H.; Kim, H. Y.; Cho, M. H.; Whangbo, M. H.; Yoo, K. H.; Kim, S. J. Hydrogen sensing under ambient conditions using SnO_2 nanowires: synergetic effect of Pd/Sn codeposition. *Nano Lett.* **2013**, *13*, 5938−5943.

(17) Zhou, W.; Dai, X.; Fu, T. M.; Xie, C.; Liu, J.; Lieber, C. M. Long term stability of nanowire nanoelectronics in physiological environments. *Nano Lett.* **2014**, *14*, 1614−1619.

(18) Na, J.; Huh, J.; Park, S. C.; Kim, D.; Kim, D. W.; Lee, J. W.; Hwang, I.-S.; Lee, J.-H.; Ha, J. S.; Kim, G. T. Degradation pattern of SnO_2 nanowire field effect transistors. *Nanotechnology* **2010**, *21*, 485201.

(19) Hong, W.-K. Aging-dependent electrical properties in polymer-passivated ZnO nanowire field effect transistors. *ECS Solid State Lett.* **2015**, *4*, Q17−Q20.

DOI: 10.1021/acssensors.7b00716
ACS Sens. 2017, 2, 1854−1859

(20) Lim, T.; Bong, J.; Mills, E. M.; Kim, S.; Ju, S. Highly stable operation of metal oxide nanowire transistors in ambient humidity, water, blood, and oxygen. *ACS Appl. Mater. Interfaces* **2015**, *7*, 16296−16302.
(21) Simpkins, B. S.; Mastro, M. A.; Eddy, C. R.; Pehrsson, P. E. Surface depletion effects in semiconducting nanowires. *J. Appl. Phys.* **2008**, *103*, 104313.
(22) Calahorra, Y.; Yalon, E.; Ritter, D. On the diameter dependence of metal-nanowire schottky barrier height. *J. Appl. Phys.* **2015**, *117*, 034308.
(23) Leonard, F.; Talin, A. A. Size-dependent effects on electrical contacts to nanotubes and nanowires. *Phys. Rev. Lett.* **2006**, *97*, 026804.
(24) Ford, A. C.; Ho, J. C.; Chueh, Y.-L.; Tseng, Y.-C.; Fan, Z.; Guo, J.; Bokor, J.; Javey, A. Diameter-dependent electron mobility of inas nanowires. *Nano Lett.* **2009**, *9*, 360−365.
(25) Cui, Y.; Duan, X.; Hu, J.; Lieber, C. M. Doping and electrical transport in silicon nanowires. *J. Phys. Chem. B* **2000**, *104*, 5213−5216.
(26) Kim, C. J.; Kang, K.; Woo, Y. S.; Ryu, K. G.; Moon, H.; Kim, J. M.; Zang, D. S.; Jo, M. H. Spontaneous chemical vapor growth of NiSi nanowires and their metallic properties. *Adv. Mater.* **2007**, *19*, 3637−3642.
(27) Lin, Y.-C.; Lu, K.-C.; Wu, W.-W.; Bai, J.; Chen, L. J.; Tu, K. N.; Huang, Y. Single crystalline PtSi nanowires, PtSi/Si/PtSi nanowire heterostructures, and nanodevices. *Nano Lett.* **2008**, *8*, 913−918.
(28) Weber, W. M.; Geelhaar, L.; Graham, A. P.; Unger, E.; Duesberg, G. S.; Liebau, M.; Pamler, W.; Chèze, C.; Riechert, H.; Lugli, P.; Kreupl, F. Silicon-nanowire transistors with intruded nickel-silicide contacts. *Nano Lett.* **2006**, *6*, 2660−2666.
(29) Lin, Y. F.; Jian, W. B. The impact of nanocontact on nanowire based nanoelectronics. *Nano Lett.* **2008**, *8*, 3146−3150.
(30) Kim, S.; Kim, S.; Srisungsitthisunti, P.; Lee, C.; Xu, M.; Ye, P. D.; Qi, M.; Xu, X.; Zhou, C.; Ju, S.; Janes, D. B. Selective contact anneal effects on indium oxide nanowire transistors using femtosecond laser. *J. Phys. Chem. C* **2011**, *115*, 17147−17153.
(31) Nagashima, K.; Yanagida, T.; Klamchuen, A.; Kanai, M.; Oka, K.; Seki, S.; Kawai, T. Interfacial effect on metal/oxide nanowire junctions. *Appl. Phys. Lett.* **2010**, *96*, 073110.
(32) Chen, H. T.; Xiong, S. J.; Wu, X. L.; Zhu, J.; Shen, J. C.; Chu, P. K. Tin oxide nanoribbons with vacancy structures in luminescence-sensitive oxygen sensing. *Nano Lett.* **2009**, *9*, 1926−1931.
(33) Singh, A. K.; Janotti, A.; Scheffler, M.; Van de Walle, C. G. Sources of electrical conductivity in SnO_2. *Phys. Rev. Lett.* **2008**, *101*, 055502.
(34) Kılıç, Ç.; Zunger, A. Origins of coexistence of conductivity and transparency in SnO_2. *Phys. Rev. Lett.* **2002**, *88*, 095501.
(35) Samson, S.; Fonstad, C. G. Defect structure and electronic donor levels in stannic oxide crystals. *J. Appl. Phys.* **1973**, *44*, 4618−4621.
(36) Li, H.; Robertson, J. Behaviour of hydrogen in wide band gap oxides. *J. Appl. Phys.* **2014**, *115*, 203708.
(37) Brillson, L. J.; Lu, Y. ZnO schottky barriers and ohmic contacts. *J. Appl. Phys.* **2011**, *109*, 121301.
(38) Murphy, T. E.; Blaszczak, J. O.; Moazzami, K.; Bowen, W. E.; Phillips, J. D. Properties of electrical contacts on bulk and epitaxial n-type ZnO. *J. Electron. Mater.* **2005**, *34*, 389−394.
(39) McAlpine, M. C.; Ahmad, H.; Wang, D.; Heath, J. R. Highly ordered nanowire arrays on plastic substrates for ultrasensitive flexible chemical sensors. *Nat. Mater.* **2007**, *6*, 379−384.
(40) Pantelopoulos, A.; Bourbakis, N. G. A Survey on Wearable Sensor-Based Systems for Health Monitoring and Prognosis. *IEEE Trans. Syst., Man., Cybern. C* **2010**, *40*, 1−12.
(41) Zhu, Z.; Suzuki, M.; Nagashima, K.; Yoshida, H.; Kanai, M.; Meng, G.; Anzai, H.; Zhuge, F.; He, Y.; Boudot, M.; Takeda, S.; Yanagida, T. Rational concept for reducing growth temperature in vapor-liquid-solid process of metal oxide nanowires. *Nano Lett.* **2016**, *16*, 7495−7502.
(42) Anzai, H.; Suzuki, M.; Nagashima, K.; Kanai, M.; Zhu, Z.; He, Y.; Boudot, M.; Zhang, G.; Takahashi, T.; Kanemoto, K.; Seki, T.; Shibata, N.; Yanagida, T. True Vapor−Liquid−Solid Process Suppresses Unintentional Carrier Doping of Single Crystalline Metal Oxide Nanowires. *Nano Lett.* **2017**, *17*, 4698−4705.
(43) Choi, Y.-J.; Hwang, I.-S.; Park, J.-G.; Choi, K. J.; Park, J.-H.; Lee, J.-H. Novel fabrication of an SnO_2 nanowire gas sensor with high sensitivity. *Nanotechnology* **2008**, *19*, 95508.
(44) Kolmakov, A.; Zhang, Y.; Cheng, G.; Moskovits, M. Detection of CO and O_2 using tin oxide nanowire sensors. *Adv. Mater.* **2003**, *15*, 997−1000.
(45) Liu, L. Z.; Xu, J. Q.; Wu, X. L.; Li, T. H.; Shen, J. C.; Chu, P. K. Optical identification of oxygen vacancy types in SnO_2 nanocrystals. *Appl. Phys. Lett.* **2013**, *102*, 1−5.
(46) Bignolas, J. B.; Bujor, M.; Bardolle, J. A study of the early stages of the kinetics of titanium oxidation by Auger electron spectroscopy and mirror electron microscopy. *Surf. Sci. Lett.* **1981**, *108*, L453−L459.
(47) Vaquila, I.; Passeggi, M. C. G.; Ferrón, J. Oxide stoichiometry in the early stages of titanium oxidation. *Surf. Sci.* **1993**, *292*, L795−L800.
(48) Imanishi, A.; Tsuji, E.; Nakato, Y. Dependence of the work function of TiO_2 (rutile) on crystal faces, studied by a scanning auger microprobe. *J. Phys. Chem. C* **2007**, *111*, 2128−2132.
(49) Morgan, B. J.; Watson, G. W. Intrinsic n-type defect formation in TiO_2: a comparison of rutile and anatase from GGA+U calculations. *J. Phys. Chem. C* **2010**, *114*, 2321−2328.
(50) Lin, Y.-F.; Chang, C.-H.; Hung, T.-C.; Jian, W.-B.; Tsukagoshi, K.; Wu, Y.-H.; Chang, L.; Liu, Z.; Fang, J. Nanocontact Disorder in Nanoelectronics for Modulation of Light and Gas Sensitivities. *Sci. Rep.* **2015**, *5*, 13035.

DOI: 10.1021/acssensors.7b00716
ACS Sens. 2017, 2, 1854−1859